



This is a repository copy of *Deployment strategy of intelligent omni-surface-assisted outdoor-to-indoor millimeter-wave communications*.

White Rose Research Online URL for this paper:

<https://eprints.whiterose.ac.uk/219170/>

Version: Accepted Version

Article:

Liu, Z., Chu, X. orcid.org/0000-0003-1863-6149, Lopez-Perez, D. et al. (1 more author) (2024) Deployment strategy of intelligent omni-surface-assisted outdoor-to-indoor millimeter-wave communications. *IEEE Transactions on Wireless Communications*, 23 (12). pp. 19172-19182. ISSN 1536-1276

<https://doi.org/10.1109/TWC.2024.3479919>

© 2024 The Author(s). Except as otherwise noted, this author-accepted version of a journal article published in *IEEE Transactions on Wireless Communications* is made available via the University of Sheffield Research Publications and Copyright Policy under the terms of the Creative Commons Attribution 4.0 International License (CC-BY 4.0), which permits unrestricted use, distribution and reproduction in any medium, provided the original work is properly cited. To view a copy of this licence, visit <http://creativecommons.org/licenses/by/4.0/>

Reuse

This article is distributed under the terms of the Creative Commons Attribution (CC BY) licence. This licence allows you to distribute, remix, tweak, and build upon the work, even commercially, as long as you credit the authors for the original work. More information and the full terms of the licence here:

<https://creativecommons.org/licenses/>

Takedown

If you consider content in White Rose Research Online to be in breach of UK law, please notify us by emailing eprints@whiterose.ac.uk including the URL of the record and the reason for the withdrawal request.



eprints@whiterose.ac.uk
<https://eprints.whiterose.ac.uk/>

Deployment Strategy of Intelligent Omni-surface-assisted Outdoor-to-Indoor Millimeter-wave Communications

Zhiyu Liu, Xiaoli Chu, *Senior Member, IEEE*,
David Lopez-Perez, *Senior Member, IEEE*, and Na Tang, *Member, IEEE*

Abstract—Intelligent omni-surfaces (IOSs) have been considered for assisting outdoor-to-indoor millimeter-wave (mmWave) communications. Nevertheless, the existing works have not adequately investigated how the number or the deployment locations of IOSs should be optimized for serving multiple indoor users. In this paper, we study IOS-assisted outdoor-to-indoor mmWave communications where IOSs are installed in an exterior wall of a building to refract mmWave signals from an outdoor base station (BS) to indoor users that locate among indoor blockages. Given a fixed total number of refracting elements, we formulate an optimization problem to maximize the downlink energy efficiency of the outdoor BS while satisfying the downlink data rate requirements of the indoor users by jointly optimizing the number, locations and phase shifts of IOSs and the beamforming vectors of the BS. To address the varying dimensionality and the non-convexity of the optimization problem, we decompose it into two subproblems that optimize the IOSs’ phase shifts together with the BS beamforming vectors and the number and locations of IOSs, respectively, and devise successive convex approximation and Continuous Population-Based Incremental Learning-based algorithms to solve them alternately. Simulation results demonstrate that the proposed algorithms can obtain the optimal number and locations of IOSs, resulting in significantly enhanced energy efficiency of the outdoor BS compared to benchmark schemes.

Index Terms—Beamforming, energy efficiency, intelligent omni-surface, deployment, millimeter-wave.

I. INTRODUCTION

Nowadays, with over 80% of mobile data traffic generated or terminated indoors [1], the deployment of indoor small-cell base stations (BSs) for wireless coverage faces challenges. Managing large numbers of indoor BSs and their associated wired or optical backhaul involves high costs and complexity [2]. Moreover, their performance is hindered by inter-cell interference, especially in dense deployment scenarios [3].

This work was supported in part by the Horizon Europe Research and Innovation Program under grant 101086219, the UK EPSRC grant EP/X038971/1, the Generalitat Valenciana, Spain, through the CIDEGENT PlaGenT, Grant CIDEXG/2022/17, Project iTENTE, and the action CNS2023-144333, financed by MCIN/AEI/10.13039/501100011033 and the European Union “NextGenerationEU”/PRTR.

Zhiyu Liu, Xiaoli Chu, and Na Tang are with the Department of Electronic and Electrical Engineering, The University of Sheffield, Sheffield S1 4ET, UK (e-mail: zliu160@sheffield.ac.uk; x.chu@sheffield.ac.uk; na.tang@sheffield.ac.uk).

David López-Pérez is with the Institute of Telecommunications and Media Applications, Universitat Politècnica de València, 46022 Valencia, Spain (e-mail: dr.david.lopez@ieee.org).

To address these issues, outdoor-to-indoor communication utilizing existing outdoor BSs to serve indoor users is gaining prominence as a promising alternative solution to meet indoor mobile service demand [4], [5]. Simultaneously, the rise of millimeter-wave (mmWave) communications is anticipated to play a crucial role in 5G and future 6G mobile networks [6].

Recent studies on outdoor-to-indoor mmWave communications mainly aimed to mitigate severe penetration losses and attenuations experienced by mmWave signals propagating through walls, windows, or other building materials [2], [7]–[9]. It was shown in [10] that a relay-aided outdoor-to-indoor mmWave downlink system achieved a higher indoor coverage probability than systems without relays. In [2], outdoor-to-indoor penetration losses were addressed by deploying customer premise equipment (CPE), comprising a pair of connected outdoor and indoor units. The outdoor unit, installed on an exterior window or wall, receives mmWave signals from an outdoor BS, while the indoor unit down-converts and transmits them to indoor users. However, the deployment and maintenance of CPE, involving signal frequency conversion and active components, can be costly and power-consuming [2]. In [11], the authors focused on maximizing the downlink received signal-to-noise ratio (SNR) by jointly optimizing the active and passive beamforming of both an outdoor and an indoor hybrid reconfigurable intelligent surface (RIS). These RISs sequentially reflect an outdoor mmWave signal to an indoor receiver. We note that the study in [11] did not consider penetration losses through building materials and the reflections by two RISs will result in severe attenuation of the signal strength.

Different from RISs, intelligent omni-surfaces (IOSs) that can refract and/or reflect incident signals by changing their phase and amplitude have recently emerged [12]–[14]. An IOS is typically a planar array of nearly passive reconfigurable elements. Recent works explored the idea of installing IOSs on the exterior walls of buildings to refract signals from an outdoor BS to indoor users [12], [14]. The authors in [15] designed new IOS elements and arranged them in a hexagonal lattice structure. Simulation results showed that substituting a part of a wall with an IOS can improve the coverage probability for the outdoor-to-indoor mmWave communication system. In [16], simulation results demonstrated that replacing a part of a concrete wall with a refracting RIS that refracts

the mmWave signals from an outdoor BS to indoor users can significantly increase the coverage probability as compared with a relay-aided counterpart. The authors in [17] maximized the downlink data rate in an IOS-assisted outdoor-to-indoor mmWave cellular network by jointly optimizing the precoding matrices of both the BS and the IOS. In [18], analytical results showed that, for a fixed total number of reconfigurable elements, distributing them to multiple small IOSs evenly spaced at the same height on a selected wall resulted in a higher indoor coverage probability than deploying one large IOS on the same wall. This performance gap became more evident for a higher indoor blockage density and/or a lower SNR threshold. We note that, [16] and [17] limited their focus to a single IOS, and neither [16] nor [18] considered multi-user interference. Additionally, the optimization of both the quantity and placements of IOSs was overlooked in these studies.

In this paper, we study an outdoor-to-indoor mmWave communication system, where an outdoor BS transmits mmWave signals to indoor users through multiple IOSs deployed on the exterior wall between the BS and the users¹, taking into account the impact of indoor blockages. Our goal is to maximize the transmission energy efficiency of the outdoor BS by investigating whether a fixed number of passive elements should be distributed across a large number of small IOSs or centralized in a small number of large IOSs, while maintaining reliable downlink communications for all indoor users.

The contributions of this paper can be summarized as follows:

- We formulate an optimization problem to maximize the transmission energy efficiency of the outdoor BS while ensuring that the downlink data rate of each user remains above a threshold. This optimization problem involves a joint optimization of the number, positions, and phase shifts of the IOSs, as well as the beamforming vectors of the BS. The challenges in solving this problem primarily arise from the intricate coupling of variables, the non-convexity, and the varying dimensionality of the problem. This is distinct from the existing works that considered only a single IOS [12], [13], [15]–[17], or where the number or locations of IOSs were not optimized [12], [13], [15]–[18].
- We address the varying dimensionality of the joint optimization problem by decomposing it into two subproblems. The first subproblem involves optimizing the phase shifts of the IOSs and the beamforming vectors of the BS for a given number and locations of IOSs. For this non-convex subproblem, we devise an Energy Efficiency Maximization (EEM) algorithm to solve it by iteratively optimizing the phase shifts of each IOS and the beamforming vector of the BS. The second subproblem involves optimizing the number and locations of IOSs for

¹Since the IOSs in our system model are mainly used to refract the outdoor BS's signals to indoor users, they can also be referred to as reconfigurable refractive surfaces [14].

a given set of phase shifts and beamforming vectors, and is solved by leveraging the Continuous Population-Based Incremental Learning (PBILc) algorithm. By solving the above two subproblems alternately, we propose the IOS Locations and Number (IOSLN) Algorithm to iteratively determine the optimal quantity, placement, and phase shifts of the IOSs, alongside the beamforming vectors for the BS. It achieves this through a repeated process that alternates between the PBILc algorithm and the proposed EEM algorithm. This iterative approach ensures that the adjustments to the number and locations of IOSs directly influence their phase shifts and the BS's beamforming strategy, enabling a harmonized optimization of all the variables toward a maximized transmission energy efficiency of the outdoor BS.

- Our simulation results demonstrate that the proposed algorithms can identify suitable numbers and deployment locations of IOSs that maximize the energy efficiency of the outdoor BS, while maintaining reliable downlink communications for all indoor users. The results also indicate that, for a fixed total number of reconfigurable elements, the optimized number and locations of IOSs lead to higher energy efficiency of the BS compared to either centralized or evenly distributed IOS deployment. The optimal number of IOSs increases with the number of indoor users, and the optimized IOS locations cluster in a vertical central area of the wall.

The rest of the paper is organized as follows. In Section II, we introduce the system model and the channel model. In Section III, we formulate the BS's downlink transmission energy efficiency maximization problem and propose algorithms to solve it. Section IV presents simulation results. Finally, we conclude the paper in Section V.

II. SYSTEM MODEL

As shown in Fig. 1, we consider an outdoor-to-indoor mmWave communication system, where an outdoor BS transmits signals to K indoor users through I IOSs deployed on the wall between the BS and the users. The BS is equipped with a uniform linear array (ULA) of $M(> 1)$ antennas.

The K users are distributed on the floor of a room, which has a length of L_r , width of W_r , and height of H_r along the x-axis, y-axis and z-axis in Fig. 1, respectively. Each user is equipped with a single directional antenna. The locations of the users are denoted by $\mathbf{q}_{UE} = [q_1, \dots, q_K]$, where $q_k = (x_k, y_k, z_k)$ is the location of the k -th user, x_k and y_k follow a distribution Ξ on the 2D horizontal plane, e.g., a uniform distribution, and z_k is the k -th user's height that follows an independent uniform distribution from 1m to 2m. In the room, there are R static blockages that are distributed on the floor following a 2D homogeneous Poisson point process (PPP) with a density of κ blockage/m² [20]. We assume that the blockages are cubes with lengths $\mathbf{L}_o = [L_{o1}, \dots, L_{oR}]$, widths $\mathbf{W}_o = [W_{o1}, \dots, W_{oR}]$, and heights $\mathbf{H}_o = [H_{o1}, \dots, H_{oR}]$, where the elements of \mathbf{L}_o and \mathbf{W}_o follow independent uniform distributions from 1m to 2m,

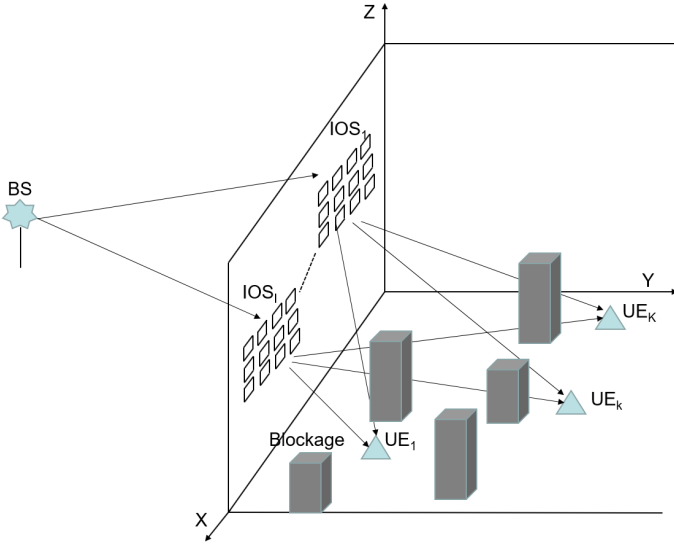


Fig. 1: An IOS-assisted outdoor-to-indoor mmWave communication system.

and those of \mathbf{H}_o in the range $[1.5\text{m}, H_r]$. Each IOS contains N elements that form a uniform rectangular array (URA). The locations of the IOSs are denoted by $\mathbf{q}_{\text{IOS}} = [\mathbf{q}_1, \dots, \mathbf{q}_I]$, where $\mathbf{q}_i = [q_{i1}, \dots, q_{iN}]$ contains the locations of the N elements on the i -th IOS, $q_{in} = (x_{in}, y_{in}, z_{in})$. For simplicity in optimizing the locations of the IOSs, the location of the central element of an IOS's array is used to present the location of the IOS, which is denoted by $q_{c_i} = (x_{c_i}, y_{c_i}, z_{c_i})$ for the i -th IOS, $i \in \{1, \dots, I\}$, with $\mathbf{q}_{\text{IOS}_c} = [q_{c_1}, \dots, q_{c_I}]$. Each IOS is connected to a smart controller that adjusts its phase shifts and refraction amplitudes via a separate wired link.

A. Channel Model

The channel from the BS to the i -th IOS is modeled as a Rician channel, and is denoted by $\mathbf{G}_i \in \mathbb{C}^{N \times M}$. The (n, m) -th element in \mathbf{G}_i denotes the channel between the m -th antenna at the BS and the n -th element on the i -th IOS, and is given by [19]

$$G_{i,mn} = \sqrt{\frac{\epsilon}{1+\epsilon}} G_{i,mn}^{\text{LoS}} + \sqrt{\frac{1}{1+\epsilon}} G_{i,mn}^{\text{NLoS}} \quad (1)$$

where ϵ is the Rician factor, $G_{i,mn}^{\text{LoS}}$ and $G_{i,mn}^{\text{NLoS}}$ are the LoS and NLoS components, respectively, and $G_{i,mn}^{\text{LoS}}$ is given by [19]

$$G_{i,mn}^{\text{LoS}} = \frac{\sqrt{J_m^{\text{BS}} J_{i,n}^{\text{IOS}} K_{i,mn}^A K_{i,mn}^D} e^{\left(\frac{-j2\pi d_{i,mn}}{\lambda}\right)}}{(4\pi)^{\frac{3}{4}} (d_{i,mn})^\alpha} \quad (2)$$

where J_m^{BS} and $J_{i,n}^{\text{IOS}}$ are the maximum antenna gain of the m -th antenna element at the BS and the maximum antenna gain of the n -th element on the i -th IOS, respectively, $d_{i,mn} = \sqrt{(x_m - x_{in})^2 + (y_m - y_{in})^2 + (z_m - z_{in})^2}$ is the distance between the m -th antenna at the BS and the n -th element on the i -th IOS, λ is the signal wavelength, α is

the path loss exponent, $K_{i,mn}^D$ and $K_{i,mn}^A$ are the normalized radiation pattern of the m -th antenna element at the BS in the direction of the n -th element on the i -th IOS and the normalized radiation pattern of the n -th element on the i -th IOS in the direction of the m -th antenna at the BS, and are given by

$$K_{i,mn}^D = |\cos^3 \phi_{i,mn}^D|, \quad (3)$$

$$K_{i,mn}^A = |\cos^3 \phi_{i,mn}^A|, \quad (4)$$

where $\phi_{i,mn}^D$ and $\phi_{i,mn}^A$ are the angle of departure (AoD) from the m -th antenna at the BS to the n -th element on the i -th IOS and the angle of arrival (AoA) at the n -th element on the i -th IOS from the m -th antenna at the BS, respectively.

The NLoS component in (1) is given by

$$G_{i,mn}^{\text{NLoS}} = \tilde{h}_{i,mn}, \quad (5)$$

where $\tilde{h}_{i,mn} \sim \mathcal{CN}(0, 1)$ follows independent complex Gaussian distribution with zero mean and unit variance.

The channel from the i -th IOS to the k -th user is given by

$$\hat{\mathbf{h}}_{ik} = \mathbf{b}_{ik} \odot \mathbf{h}_{ik}, \quad (6)$$

where \odot denotes the element-wise multiplication, $\mathbf{b}_{ik} = [b_{ik,1}, \dots, b_{ik,N}]$ contains N binary indicators, where $b_{ik,n} = 1$ indicates that the link between the n -th element of the i -th IOS and the k -th user is LoS [16], otherwise $b_{ik,n} = 0$, and $\mathbf{h}_{ik} = [h_{ik,1}, \dots, h_{ik,N}]$, where $h_{ik,n}$ is the channel coefficient between the n -th element on the i -th IOS and the k -th user, and is given by [19]

$$h_{ik,n} = \sqrt{\frac{\epsilon}{1+\epsilon}} h_{ik,n}^{\text{LoS}} + \sqrt{\frac{1}{1+\epsilon}} h_{ik,n}^{\text{NLoS}}, \quad (7)$$

where $h_{ik,n}^{\text{LoS}}$ is the LoS component and is given by

$$h_{ik,n}^{\text{LoS}} = \frac{\lambda \sqrt{J_{i,n}^{\text{IOS}} J_k K_{ik,n}^D K_{ik,n}^A \delta_x \delta_z \gamma_{n,i}} e^{\left(\frac{-j2\pi d_{ik,n}}{\lambda}\right)}}{(4\pi)^{\frac{3}{4}} (d_{ik,n})^\alpha}, \quad (8)$$

where J_k is the maximum antenna gain of the k -th user, δ_x and δ_z are the sizes of each element on the respective IOSs, $\gamma_{n,i}$ is the power ratio between the signal re-emitted by the n -th element of the i -th IOS and the incident signal, $d_{ik,n} = \sqrt{(x_{in} - x_k)^2 + (y_{in} - y_k)^2 + (z_{in} - z_k)^2}$ is the distance between the n -th element on the i -th IOS and the k -th user, $K_{ik,n}^D$ and $K_{ik,n}^A$ are the normalized radiation pattern of the n -th element on the i -th IOS in the direction of the k -th user and the normalized radiation pattern of the k -th user's antenna, and are given by

$$K_{ik,n}^D = |\cos^3 \phi_{ik,n}^D|, \quad (9)$$

$$K_{ik,n}^A = |\cos^3 \phi_{ik,n}^A|, \quad (10)$$

where $\phi_{ik,n}^D$ and $\phi_{ik,n}^A$ are the AoD from the n -th element on the i -th IOS to the k -th user and the AoA at the k -th user from the n -th element on the i -th IOS, respectively.

The NLoS component in (7) is given by

$$h_{ik,n}^{\text{NLoS}} = \tilde{h}_{ik,n}, \quad (11)$$

where $\tilde{h}_{ik,n} \sim \mathcal{CN}(0, 1)$.

The LoS probability of the link between the n -th element on the i -th IOS and the k -th user is given by [16]

$$P_{ik,n} = \Pr[b_{ik,n} = 1] = \Gamma(z_{in})e^{-(\beta\hat{d}_{ik,n}+p)}, \quad (12)$$

where $\Gamma(z_{i,n})$ is given by

$$\Gamma(z_{i,n}) = \frac{1}{2} \times \left(1 + \frac{z_{i,n} - \mathbb{E}[\mathbf{H}_o]}{H_r} \right), \quad (13)$$

where $\mathbb{E}[\mathbf{H}_o]$ is the average height of the blockages, $\hat{d}_{ik,n} = \sqrt{(x_{in} - x_k)^2 + (y_{in} - y_k)^2}$ is the horizontal distance between the n -th element on the i -th IOS and the k -th user, and β is given by

$$\beta = \frac{2\kappa(\mathbb{E}[\mathbf{L}_o] + \mathbb{E}[\mathbf{W}_o])}{\pi}, \quad (14)$$

where κ blockages/m² is the density of blockages, $\mathbb{E}[\mathbf{L}_o]$ and $\mathbb{E}[\mathbf{W}_o]$ are the average length and width of the blockages, respectively, p in (12) is the fraction of the room's floor area covered by blockages and is given by

$$p = \kappa \mathbb{E}[\mathbf{L}_o] \mathbb{E}[\mathbf{W}_o]. \quad (15)$$

B. Downlink data rate

The signal received at the k -th user is given by

$$y_k = \left(\sum_{i=1}^I \hat{h}_{ik} \Theta_i \mathbf{G}_i \right) \mathbf{w}_k s_k + \iota_k \quad (16)$$

where $k = 1, \dots, K$, $\Theta_i = \text{diag}(e^{j\theta_{i1}}, \dots, e^{j\theta_{iN}})$ is a N -by- N diagonal matrix, θ_{in} is the refraction phase shift applied by the n -th element on the i -th IOS, s_k is the information symbol with a zero mean and unit variance (i.e., normalized power) transmitted by the BS to the k -th user, $\mathbf{w}_k \in \mathbb{C}^{M \times 1}$ is the BS beamforming vector towards the k -th user, and $\sum_{k=1}^K \mathbf{w}_k^H \mathbf{w}_k = P_T$, where P_T is the transmit power at the BS, and ι_k is the additive white Gaussian noise (AWGN) at the k -th user with zero mean and the variance of σ^2 . For analytical tractability, we assume that the IOSs' phase shifts are continuous. The results of this work can be applied to a system where the IOS phase shifts are of discrete values by adding a quantization process, which approximates the optimal continuous phase shifts of the IOS by the closest possible discrete phase shift values.

The downlink data rate at the k -th user is given by

$$r_k = B \log_2 \left(1 + \frac{\left| \left(\sum_{i=1}^I \hat{h}_{ik} \Theta_i \mathbf{G}_i \right) \mathbf{w}_k \right|^2}{\sum_{j=1, j \neq k}^K \left| \left(\sum_{i=1}^I \hat{h}_{ij} \Theta_i \mathbf{G}_i \right) \mathbf{w}_j \right|^2 + \sigma^2} \right), \quad (17)$$

where B is the bandwidth of the BS transmission to a single user.

Letting $\hat{\mathbf{h}}_k = [\hat{h}_{1k}, \dots, \hat{h}_{Ik}]$, $\mathbf{G} = [\mathbf{G}_1, \dots, \mathbf{G}_I]^H$, and $\mathbf{\Lambda} = [\mathbf{\Lambda}_1, \dots, \mathbf{\Lambda}_I]^H \in \mathbb{C}^{IN \times 1}$, where $\mathbf{\Lambda}_i =$

$[e^{j\theta_{i1}}, \dots, e^{j\theta_{iN}}]^H \in \mathbb{C}^{N \times 1}$, $\mathbf{\Lambda}_{in} = e^{j\theta_{in}}$, $\hat{\mathbf{\Theta}} = \text{diag}(\mathbf{\Lambda}) \in \mathbb{C}^{IN \times IN}$, the expression of r_k is rewritten as

$$r_k = B \log_2 \left(1 + \frac{\left| \left(\hat{\mathbf{h}}_k \hat{\mathbf{\Theta}} \mathbf{G} \right) \mathbf{w}_k \right|^2}{\sum_{j=1, j \neq k}^K \left| \left(\hat{\mathbf{h}}_k \hat{\mathbf{\Theta}} \mathbf{G} \right) \mathbf{w}_j \right|^2 + \sigma^2} \right). \quad (18)$$

III. PROBLEM FORMULATION AND SOLUTION ALGORITHMS

A. Problem Formulation

We formulate an optimization problem to maximize the downlink transmission energy efficiency of the BS by jointly optimizing the number and locations of IOSs, the refraction phase shifts of all the IOS elements, and the beamforming vectors of the BS, subject to the constraints on the downlink data rate of each user and the maximum transmission power of the BS, i.e.,

$$(P1) : \max_{I, \mathbf{q}_{\text{IOS}_c}, \hat{\mathbf{\Theta}}, \mathbf{w}_1, \dots, \mathbf{w}_K} \frac{\sum_{k=1}^K r_k}{\sum_{k=1}^K \mathbf{w}_k^H \mathbf{w}_k + P_C} \quad (19)$$

$$\text{s.t. } C1 : \sum_{k=1}^K \mathbf{w}_k^H \mathbf{w}_k \leq P_{T \max}, \quad (19a)$$

$$C2 : 0 \leq \theta_{in} < 2\pi, \forall i, \forall n, \quad (19b)$$

$$C3 : r_k \geq r_{\min, k}, \forall k, \quad (19c)$$

$$C4 : I \geq 1, \quad (19d)$$

$$C5 : \frac{d_I}{2} \leq x_{ci} \leq L_r - \frac{d_I}{2}, \forall i, \quad (19e)$$

$$C6 : \mathbb{E}[\mathbf{H}_o] + \frac{d_I}{2} \leq z_{ci} \leq H_r - \frac{d_I}{2}, \forall i, \quad (19f)$$

$$C7 : |z_{ci} - z_{cj}| \geq d_I, \text{ or } |x_{ci} - x_{cj}| \geq d_I, i \neq j, \forall i, \forall j, \quad (19g)$$

where I is the number of IOSs and $\mathbf{q}_{\text{IOS}_c}$ contains the locations of the IOSs, $P_{T \max}$ is the maximum transmit power of the BS, $r_{\min, k}$ is the minimum downlink data rate required by the k -th user, d_I is the size of an IOS, and the minimum distance we set between two IOSs to avoid overlapping, P_C denotes the total power consumed by the active transceivers at the BS and by the circuits of the BS and the users, and it is given by [22]

$$P_C = P_{BS} + N_{TR} P_{TR} + \sum_{k=1}^K P_k, \quad (20)$$

where P_{BS} is the circuit power consumed by the BS, N_{TR} is the number of active transceivers at the BS, P_{TR} is the power consumed by each active transceiver at the BS, and P_k is the circuit power consumed by the k -th user. In (P1), constraint C1 specifies the maximum transmit power at the outdoor BS, C2 imposes the value range of the phase shift for each element on the IOSs, C3 ensures that the downlink data rate at each user is above the minimum downlink data rate required, C4 guarantees that at least one IOS is deployed, C5 and C6 delineate the permissible spatial boundaries for the placement of IOSs, and C7 precludes the overlap of these IOSs, ensuring their distinct and non-intersecting distribution.

B. EEM Algorithm

We note that it is hard to solve (P1) directly due to the varying number of variables involved and its non-convexity. Hence, we first study the case with the number I and the locations of IOSs fixed, for which (P1) reduces to

$$(P2) : \max_{\hat{\Theta}, \mathbf{w}_1, \dots, \mathbf{w}_K} \frac{\sum_{k=1}^K r_k}{\sum_{k=1}^K \mathbf{w}_k^H \mathbf{w}_k + P_C} \quad (21)$$

s.t. C1, C2, C3.

Since (P2) is still a non-convex problem and is difficult to solve directly, we decompose (P2) into two subproblems that optimize the IOSs' refraction phase shifts for given beamforming vectors of the BS and the BS's beamforming vectors for given refraction phase shifts of the IOSs, respectively.

1) Refraction phase shifts:

For given beamforming vector $\mathbf{w}_k, k = 1, \dots, K$, (P2) reduces to

$$(P3) : \max_{\hat{\Theta}, \boldsymbol{\eta}} \sum_{k=1}^K \log_2(1 + \eta_k) \quad (22)$$

s.t.

$$C2$$

$$C8 : \eta_k \leq \frac{\left| \left(\hat{\mathbf{h}}_k \hat{\Theta} \mathbf{G} \right) \mathbf{w}_k \right|^2}{\sum_{j=1, j \neq k}^K \left| \left(\hat{\mathbf{h}}_k \hat{\Theta} \mathbf{G} \right) \mathbf{w}_j \right|^2 + \sigma^2}, \quad (22a)$$

$\forall k \in \{1, \dots, K\}$,

$$C9 : \eta_k \geq 2^{\frac{r_{\min, k}}{B}} - 1, \quad \forall k \in \{1, \dots, K\}. \quad (22b)$$

where $\boldsymbol{\eta} = [\eta_1, \dots, \eta_K] \in \mathbb{C}^{1 \times K}$ is a slack vector that returns the optimal solution when the equality in constraint C8 holds, and C9 ensures the minimum rate required of each user. Letting $\left(\hat{\mathbf{h}}_k \hat{\Theta} \mathbf{G} \right) \mathbf{w}_j = \boldsymbol{\varsigma}_{kj}^H \boldsymbol{\Lambda}$, where $\boldsymbol{\varsigma}_{kj} = \text{diag} \left(\hat{\mathbf{h}}_k \right) \mathbf{G} \mathbf{w}_j$, C8 can be rewritten as

$$C8' : \eta_k \leq \frac{\left| \boldsymbol{\varsigma}_{kk}^H \boldsymbol{\Lambda} \right|^2}{\sum_{j=1, j \neq k}^K \left| \boldsymbol{\varsigma}_{kj}^H \boldsymbol{\Lambda} \right|^2 + \sigma^2}, \quad \forall k \in \{1, \dots, K\}. \quad (23)$$

To deal with the non-convexity of C8', we introduce the auxiliary variables $\zeta_k, k = 1, \dots, K$, $\boldsymbol{\zeta} = [\zeta_1, \dots, \zeta_K]$, and convert C8' to C8.1' and C8.2' as follows

$$C8.1' : \left| \boldsymbol{\varsigma}_{kk}^H \boldsymbol{\Lambda} \right|^2 \geq \zeta_k \eta_k = \frac{1}{4} \left((\zeta_k + \eta_k)^2 - (\zeta_k - \eta_k)^2 \right), \quad (24)$$

$$C8.2' : \sum_{j=1, j \neq k}^K \left| \boldsymbol{\varsigma}_{kj}^H \boldsymbol{\Lambda} \right|^2 + \sigma^2 \leq \zeta_k, \quad (25)$$

By substituting C8.1' and C8.2' into (P3), we have

$$(P4) : \max_{\boldsymbol{\Lambda}, \boldsymbol{\eta}, \boldsymbol{\zeta}} \sum_{k=1}^K \log_2(1 + \eta_k) \quad (26)$$

s.t.

$$C8.1', C8.2', C9$$

$$C2' : \left| \Lambda_{in} \right| = 1, \quad \forall i \in \{1, \dots, I\}, \forall n \in \{1, \dots, N\}. \quad (26a)$$

$$C10 : \zeta_k \geq 0, \quad \forall k \in \{1, \dots, K\}. \quad (26b)$$

By applying the penalty method, (P4) can be rewritten as

$$(P5) : \max_{\boldsymbol{\Lambda}, \boldsymbol{\eta}, \boldsymbol{\zeta}} \sum_{k=1}^K \log_2(1 + \eta_k) + A \sum_{i=1}^I \sum_{n=1}^N (|\Lambda_{in}|^2 - 1) \quad (27)$$

s.t.

$$C8.1', C8.2', C9, C10,$$

$$C2'' : \left| \Lambda_{in} \right| \leq 1, \quad \forall i \in \{1, \dots, I\}, \forall n \in \{1, \dots, N\}. \quad (27a)$$

where A is a positive constant, and the optimal solution will be achieved when $|\Lambda_{in}| = 1, \forall i \in \{1, \dots, I\}, \forall n \in \{1, \dots, N\}$.

Then, we use successive convex approximation (SCA) to solve (P5) iteratively as follows. In the s -th iteration, where $s \geq 1$, the objective function of (P5) is approximated by

$$\max_{\boldsymbol{\Lambda}, \boldsymbol{\eta}, \boldsymbol{\zeta}} \sum_{k=1}^K \log_2 \left(1 + \eta_k^{(s)} \right) + 2A \sum_{i=1}^I \sum_{n=1}^N \Lambda_{in}^{(s-1)} \left(\Lambda_{in}^{(s)} - \Lambda_{in}^{(s-1)} \right) \quad (28)$$

where $2A \sum_{i=1}^I \sum_{n=1}^N \Lambda_{in}^{(s-1)} \left(\Lambda_{in}^{(s)} - \Lambda_{in}^{(s-1)} \right)$ is the first order Taylor polynomial of $A \sum_{i=1}^I \sum_{n=1}^N \left(\left| \Lambda_{in}^{(s)} \right|^2 - 1 \right)$ at $\Lambda_{in}^{(s-1)}$, and $\Lambda_{in}^{(0)}$ is the initial value of Λ_{in} .

Although C8.2' is convex, C8.1' is still non-convex. Since $\left| \boldsymbol{\varsigma}_{kk}^H \boldsymbol{\Lambda} \right|^2$ and $(\zeta_k - \eta_k)^2$ are convex and any convex function is globally lower-bounded by its first order Taylor polynomial at any point [23], we approximate both sides of C8.1' by their first order Taylor polynomial at $\boldsymbol{\Lambda}^{(s-1)}$, $\zeta_k^{(s-1)}$, and $\eta_k^{(s-1)}$ and have

$$C8.1'' : 2\Re \left(\left(\boldsymbol{\varsigma}_{kk}^H \boldsymbol{\Lambda}^{(s-1)} \right)^H \boldsymbol{\varsigma}_{kk}^H \boldsymbol{\Lambda}^{(s)} \right) - \left| \boldsymbol{\varsigma}_{kk}^H \boldsymbol{\Lambda}^{(s-1)} \right|^2 \geq \frac{1}{4} \left[\left(\zeta_k^{(s)} + \eta_k^{(s)} \right)^2 - \left(\zeta_k^{(s-1)} - \eta_k^{(s-1)} \right) \left(\zeta_k^{(s)} - \eta_k^{(s)} \right) + \left(\zeta_k^{(s-1)} - \eta_k^{(s-1)} \right)^2 \right]. \quad (29)$$

Based on (28) and (29), (P5) can be approximated to the following convex problem:

$$(P6) : \max_{\boldsymbol{\Lambda}^{(s)}, \boldsymbol{\eta}^{(s)}, \boldsymbol{\zeta}^{(s)}} \sum_{k=1}^K \log_2 \left(1 + \eta_k^{(s)} \right) + 2A \sum_{i=1}^I \sum_{n=1}^N \Lambda_{in}^{(s-1)} \left(\Lambda_{in}^{(s)} - \Lambda_{in}^{(s-1)} \right) \quad (30)$$

$$s.t. \quad C8.2', C8.1'', C9, C2'', C10.$$

Since (P6) is a convex problem, it can be solved by the CVX toolbox [26]. With the optimal $\boldsymbol{\Lambda}$ obtained by solving (P6), we have the optimal $\hat{\Theta}$.

2) Beamforming vector:

Continuing from the previous subsection, with the $\hat{\Theta}$ obtained by solving (P6), (P2) reduces to

$$(P7) : \max_{\tilde{\boldsymbol{\eta}}, \mathbf{w}_1, \dots, \mathbf{w}_K} \frac{\sum_{k=1}^K B \log_2(1 + \tilde{\eta}_k)}{\sum_{k=1}^K \mathbf{w}_k^H \mathbf{w}_k + P_C} \quad (31)$$

s.t.

C1,

$$C11: \tilde{\eta}_k \leq \frac{|\tilde{\zeta}_k^H \mathbf{w}_k|^2}{\sum_{j=1, j \neq k}^K |\tilde{\zeta}_k^H \mathbf{w}_j|^2 + \sigma^2}, \forall k \in \{1, \dots, K\}, \quad (31a)$$

$$C12: \tilde{\eta}_k \geq 2^{\frac{r_{\min, k}}{B}} - 1, \forall k \in \{1, \dots, K\}, \quad (31b)$$

where $\tilde{\boldsymbol{\eta}} = [\tilde{\eta}_1, \dots, \tilde{\eta}_K]$ contains K slack variables, and $\tilde{\zeta}_k = \hat{\mathbf{h}}_k \hat{\mathbf{G}}$.

To deal with the non-convexity of $C11$, we introduce the slack variable $\tilde{\zeta}_k > 0$, $k = 1, \dots, K$, $\tilde{\boldsymbol{\zeta}} = [\tilde{\zeta}_1, \dots, \tilde{\zeta}_K]$. Since we can express $\tilde{\zeta}_k^H \mathbf{w}_k$ as a real number by arbitrarily rotating the phase of \mathbf{w}_k [21], we convert $C11$ to

$$C11.1: \sqrt{\tilde{\eta}_k \tilde{\zeta}_k} \leq \Re(\tilde{\zeta}_k^H \mathbf{w}_k), \quad (32)$$

$$C11.2: \sum_{j=1, j \neq k}^K |\tilde{\zeta}_k^H \mathbf{w}_j|^2 + \sigma^2 \leq \tilde{\zeta}_k. \quad (33)$$

Since $C11.1$ is still non-convex, we apply SCA to it, i.e., by substituting $\sqrt{\tilde{\eta}_k \tilde{\zeta}_k}$ with its first order Taylor polynomial, and in the s -th iteration we have

$$\begin{aligned} C11.1': \Re\left(\tilde{\zeta}_k^{(s)} \mathbf{w}_k^{(s)H}\right) &\geq \sqrt{\tilde{\eta}_k^{(s-1)} \tilde{\zeta}_k^{(s-1)}} \\ &+ \frac{1}{2} \sqrt{\frac{\tilde{\zeta}_k^{(s-1)}}{\tilde{\eta}_k^{(s-1)}}} \left(\tilde{\eta}_k^{(s)} - \tilde{\eta}_k^{(s-1)}\right) \\ &+ \frac{1}{2} \sqrt{\frac{\tilde{\eta}_k^{(s-1)}}{\tilde{\zeta}_k^{(s-1)}}} \left(\tilde{\zeta}_k^{(s)} - \tilde{\zeta}_k^{(s-1)}\right). \end{aligned} \quad (34)$$

Replacing $C11$ by $C11.1'$ and $C11.2$, (P7) converts to

$$(P8): \max_{\tilde{\boldsymbol{\eta}}^{(s)}, \mathbf{w}_1^{(s)}, \dots, \mathbf{w}_K^{(s)}, \tilde{\boldsymbol{\zeta}}^{(s)}} \frac{\sum_{k=1}^K B \log_2(1 + \tilde{\eta}_k^{(s)})}{\sum_{k=1}^K \mathbf{w}_k^{(s)H} \mathbf{w}_k^{(s)} + P_C} \quad (35)$$

s.t. $C1, C11.1', C11.2, C12$.

We note that (P8) is a convex problem and can be solved by the Dinkelbach method [24].

Algorithm 1 EEM Algorithm

Input: $\hat{\mathbf{h}}_k, \forall k \in \{1, \dots, K\}, \mathbf{G}, I, \mathbf{q}_I, \varepsilon$

Output: $\hat{\boldsymbol{\Theta}}_{\text{opt}}, \mathbf{w}_{1\text{opt}}, \dots, \mathbf{w}_{K\text{opt}}, EE_{\text{opt}}$

- 1: Set the iteration index $s = 0$ and initialize $\hat{\boldsymbol{\Theta}}^{(0)}, \mathbf{w}_k^{(0)}$ and $EE^{(0)} \forall k \in \{1, \dots, K\}$.
 - 2: **repeat**
 - 3: Update $s = s + 1$.
 - 4: Obtain $\hat{\boldsymbol{\Theta}}^{(s)}$ by solving (P6).
 - 5: Obtain $\mathbf{w}_k^{(s)}, \forall k \in \{1, \dots, K\}$ by solving (P8).
 - 6: Obtain $EE^{(s)}$ by calculating (21).
 - 7: **until** $EE^{(s)} - EE^{(s-1)} < \varepsilon$.
 - 8: $EE_{\text{opt}} = EE^{(s)}, \hat{\boldsymbol{\Theta}}_{\text{opt}} = \hat{\boldsymbol{\Theta}}^{(s)}, \mathbf{w}_{k\text{opt}} = \mathbf{w}_k^{(s)}, \forall k \in \{1, \dots, K\}$.
-

Based on the above solutions to (P6) and (P8), we propose an iterative algorithm to solve (P2) by solving (P6) and (P8) alternately in each iteration as shown in Algorithm 1, where ε is a very small positive value used to terminate the iteration. It is not difficult to verify that the introduction of the slack variables does not lose the optimality of the optimization problem, since all the constraints that include slack variables can be met with equality.

For subproblems (P6) and (P8), the optimal solutions are obtained in each iteration of Algorithm 1, and as a result, the objective function in (P2) is non-decreasing over iterations. Moreover, the objective function of (P2) is upper bounded due to the maximum transmit power at the BS. Thus, the proposed EEM algorithm is guaranteed to converge.

The complexity of Algorithm 1 is analyzed as follows. In each iteration of Algorithm 1, the complexity of solving (P6) is $\mathcal{O}((2K + IN)^2(4K + IN))$ [25], where $2K + IN$ and $4K + IN$ are the number of variables and the total number of constraints in (P6), respectively; and the complexity of solving (P8) is $\mathcal{O}(DQ)$ [24], where D is the number of iterations required by the Dinkelbach method and Q is the complexity per iteration of the Dinkelbach method. The number of iterations required by the SCA to converge in solving (P5) is $\mathcal{O}(\sqrt{4K + IN} \log_2(1/\varepsilon))$ [26], where $4K + IN$ is the total number of constraints in (P5); while the number of iterations required by the SCA to converge in solving (P7) is $\mathcal{O}(\sqrt{2K + 1} \log_2(1/\varepsilon))$, where $2K + 1$ is the total number of constraints in (P7). So, the complexity of Algorithm 1 is $\mathcal{O}\left(\log_2(1/\varepsilon) \left[\sqrt{4K + IN} (2K + IN)^2 (4K + IN) + \sqrt{2K + 1} DQ \right]\right)$ [21].

C. IOSLN Algorithm

For given phase shifts of IOSs and beamforming vectors of the BS obtained by Algorithm 1, (P1) reduces to

$$(P9): \max_{I, \mathbf{q}_{\text{IOSc}}} \frac{\sum_{k=1}^K r_k}{\sum_{k=1}^K \mathbf{w}_k^H \mathbf{w}_k + P_C} \quad (36)$$

s.t. $C3, C4, C5, C6, C7$.

To solve (P9) is to obtain the optimal number and locations of IOSs that maximize the downlink transmission energy efficiency of the BS. To this end, we divide the wall area where the IOSs will be deployed (as defined by C5 and C6) into $\frac{L_r}{d_I}$ columns each of the same length $H_r - E[\mathbf{H}_o]$ and width d_I , where $\frac{L_r}{d_I}$ is assumed to be an integer for simplicity. This is because d_I is much smaller than L_r and we allow the outermost column at either edge of the wall to be slightly wider than d_I . Each IOS is deployed within a column (not across any two columns). More than one IOS is allowed to be deployed in a column. Without loss of generality, if one of the top corners of the wall is assigned the value of 0 and its diagonally opposite corner of the considered wall area is assigned the value of $\frac{L_r(H_r - E[\mathbf{H}_o])}{d_I}$, then all possible IOS-deployment locations on the wall form a continuous range

from 0 to $\frac{L_r(H_r-E[\mathbf{H}_o])}{d_I}$. To obtain the optimal locations of I IOSs for given I , we employ the Population Based Incremental Learning for continuous space (PBILc) [27], where a probabilistic model that characterizes a population evolves over generations instead of the individuals in the population. Hence, PBILc is more efficient than traditional evolutionary algorithms such as the genetic algorithm (GA) and particle swarm optimization (PSO).

In the following, we present the PBILc-based IOSLN algorithm to solve (P9). First, we set the number of IOS(s) $I = 1$ and the iteration index $s' = 1$, and randomly initialize a population of N_{ind} individuals, where N_{ind} is an even number and each individual contains the location(s) of I IOS(s), $\mathbf{q}_{IOS_c} = [q_{c1}, \dots, q_{cI}]$. The initialized location of each IOS follows an independent, identical Gaussian distribution $\mathcal{N}(X^{(s')}, \sigma_X^{(s')})$, where the initialized mean value $X^{(s')} = \frac{L_r(H_r-E[\mathbf{H}_o])}{2d_I}$ (i.e., the centre of the considered wall area), and the initialized standard deviation $\sigma_X^{(s')} = \frac{L_r(H_r-E[\mathbf{H}_o])}{4d_I}$. An individual will be discarded and generated again if any two of its IOS locations are in the same column and the distance between them is smaller than d_I . Then, Algorithm 1 is used to obtain $\mathbf{w}_{kopt}, \hat{\Theta}_{opt}, k \in \{1, \dots, K\}$ for each individual and EE_{opt} is taken as the fitness value of the corresponding individual. The individual with the largest fitness value in the population is identified, and its $\mathbf{w}_{kopt}, \hat{\Theta}_{opt}$ and EE_{opt} are denoted by $\mathbf{w}_{kopt}^{(s')}, \hat{\Theta}_{opt}^{(s')}$ and $EE_{opt}^{(s')}$, $k \in \{1, \dots, K\}$, respectively.

Update $s' = s' + 1$, and a new half-population of $\frac{N_{ind}}{2}$ individuals are generated by selecting the $\frac{N_{ind}}{2}$ individuals of the highest fitness values from the previous population. Next, the mean value of the Gaussian distribution is updated as

$$X^{(s')} = (1-\chi)X^{(s'-1)} + \chi(X^{best1} + X^{best2} - X^{worst}), \quad (37)$$

where $\chi \in (0, 1)$ is a constant relaxation factor, X^{best1} and X^{best2} are the mean values of the two individuals with the largest two fitness values in the new half-population, and X^{worst} is the mean value of the individual with the smallest fitness value in the new half-population. The standard deviation of the Gaussian distribution is updated as

$$\sigma_X^{(s')} = (1-\chi)\sigma_X^{(s'-1)} + \chi\sqrt{\frac{\sum_{j=1}^{\frac{N_{ind}}{2}}(X_j - \bar{X}_j)^2}{\frac{N_{ind}}{2}}}, \quad (38)$$

where X_j is the mean value of the j -th individual of the new half-population, and \bar{X}_j is the average value of all X_j , for $j = 1, \dots, \frac{N_{ind}}{2}$. Afterwards, another new half-population of $\frac{N_{ind}}{2}$ individuals are generated independently following the updated Gaussian distribution. An individual will be discarded and generated again if any two of its IOS locations are in the same column and their distance is less than d_I . The two half-populations form a new population. Then, for each individual in the new population, Algorithm 1 is used to obtain $\mathbf{w}_{kopt}, \hat{\Theta}_{opt}$ and $EE_{opt}, k \in \{1, \dots, K\}$. The individual that has the largest fitness value among the population is identified, and

its $\mathbf{w}_{kopt}, \hat{\Theta}_{opt}$ and EE_{opt} are labeled as $\mathbf{w}_{kopt}^{(s')}, \hat{\Theta}_{opt}^{(s')}$ and $EE_{opt}^{(s')}$, $k \in \{1, \dots, K\}$, respectively.

The above procedures repeat until $EE_{opt}^{(s')} - EE_{opt}^{(s'-1)} < \varepsilon$. Once the iteration terminates, the individual of the largest fitness value among the latest population is identified as the optimal locations of the I IOSs, labeled as \mathbf{q}_{optI} , and its $\mathbf{w}_{kopt}^{(s')}, \hat{\Theta}_{opt}^{(s')}$ and $EE_{opt}^{(s')}$ are labeled as $\mathbf{w}_{koptI}, \hat{\Theta}_{optI}$, and $EE_{optI}, k \in \{1, \dots, K\}$, respectively. The above iterative algorithm for any given value of I is ensured to converge when the iteration number is large enough [27].

Update $I = I + 1$ and repeat the above procedures until $EE_{optI} - EE_{opt(I-1)} < \varepsilon$. Finally, the value of I that is associated with the highest value of EE_{optI} is identified as I_{opt} and its corresponding $\mathbf{q}_{optI}, EE_{optI}, \mathbf{w}_{koptI}, \hat{\Theta}_{optI}, k \in \{1, \dots, K\}$ return the optimal IOS locations, energy efficiency of the BS, BS beamforming vectors and IOS phase shifts, respectively.

The above IOSLN Algorithm is summarized in Algorithm 2. It has a complexity of $\mathcal{O}\left(\sum_{I=1}^{I_{opt}} \left(\log_2(1/\varepsilon) \left[\sqrt{2K+IN}(2K+IN)^2(4K+IN) + \sqrt{2K+1}DQ\right] N_{ind}^{\frac{N_{PI}+1}{2}}\right)\right)$, where N_{PI} is the number of iterations required for the PBILc to converge for $I \in \{1, \dots, I_{opt}\}$.

IV. SIMULATION RESULTS

In this section, we present simulation results to evaluate the performance of the proposed algorithms. The simulated system model aligns with the description in Section II, and the parameter values used in the simulation are listed in Table I unless otherwise specified. In the simulations, we compare the performance of Algorithm 2 with three benchmark schemes: (i) an evenly distributed IOS deployment scheme [18], where the IOSs are evenly spaced on the wall at the same height, and the number and height of IOSs are optimized using Algorithm 2; (ii) centralized deployment (i.e., a single IOS) with an optimal location on the wall obtained by Algorithm 2 using $I = 1$; and (iii) the case without deploying any RIS. In all compared schemes, the IOSs are deployed on the same wall, as shown in Fig. 1, and the total number (IN) of elements on IOS(s) is kept constant.

In Fig. 2, we plot the energy efficiency of the outdoor BS versus the number of iterations in Algorithm 2 for different population sizes (N_{ind}) used in the PBILc. The energy efficiency of the outdoor BS first increases with the iteration number and finally converges to a stable value. Algorithm 2 converges faster for a larger value of N_{ind} , because it is likely to obtain a larger fitness value in each iteration with a larger population size.

In Fig. 3, we present a plot of the downlink transmission energy efficiency of the outdoor BS against the number of users in the indoor environment under consideration. The energy efficiency for all four schemes is observed to decrease as the number of users increases, given that a larger number

Algorithm 2 IOSLN Algorithm

Input: $N_{\text{ind}}, \varepsilon, K, \Xi$.

Output: $I_{\text{opt}}, \mathbf{q}_{\text{opt}I}, EE_{\text{opt}I}, \mathbf{w}_{\text{kopt}I}, \hat{\Theta}_{\text{opt}I}, k \in \{1, \dots, K\}$.

- 1: Initialize $I = 0$ and $EE_{\text{opt}0} = 0$.
 - 2: **repeat**
 - 3: Update $I = I + 1$
 - 4: Set the iteration index $s' = 1$, and randomly initialize a population of N_{ind} individuals, where each individual contains I independent IOS locations, $q_i \sim \mathcal{N}(X^{(s')}, \sigma_X^{(s')})$, $i \in \{1, \dots, I\}$, where $X^{(s')} = \frac{L_r(H_r - E[\mathbf{H}_o])}{2d_I}$ and $\sigma_X^{(s')} = \frac{L_r(H_r - E[\mathbf{H}_o])}{4d_I}$. Run Algorithm 1 for each individual and take EE_{opt} as its fitness value.
 - 5: **repeat**
 - 6: Update $s' = s' + 1$.
 - 7: A new half-population is formed by the $\frac{N_{\text{ind}}}{2}$ individuals with the largest fitness values of the previous population.
 - 8: Update $X^{(s')}$ and $\sigma_X^{(s')}$ based on (37) and (38), respectively.
 - 9: Generate $\frac{N_{\text{ind}}}{2}$ individuals independently following $\mathcal{N}(X^{(s')}, \sigma_X^{(s')})$. The two half-populations to form a new population.
 - 10: Run Algorithm 1 for each individual in the new population. The individual that has the largest fitness value returns $\mathbf{w}_{\text{kopt}I}^{(s')}, \hat{\Theta}_{\text{opt}I}^{(s')}$ and $EE_{\text{opt}I}^{(s')}$, $k \in \{1, \dots, K\}$.
 - 11: **until** $EE_{\text{opt}I}^{(s')} - EE_{\text{opt}I}^{(s'-1)} < \varepsilon$.
 - 12: $\mathbf{w}_{\text{kopt}I} = \mathbf{w}_{\text{kopt}I}^{(s')}, \hat{\Theta}_{\text{opt}I} = \hat{\Theta}_{\text{opt}I}^{(s')}, EE_{\text{opt}I} = EE_{\text{opt}I}^{(s')}$, $k \in \{1, \dots, K\}$.
 - 13: **until** $EE_{\text{opt}I} - EE_{\text{opt}(I-1)} < \varepsilon$.
 - 14: $I_{\text{opt}} = \underset{I}{\text{argmax}} \{EE_{\text{opt}I}\}$ and return its $\mathbf{q}_{I_{\text{opt}}}, EE_{\text{opt}I}, \mathbf{w}_{\text{kopt}I}, \hat{\Theta}_{\text{opt}I}, k \in \{1, \dots, K\}$ as output.
-

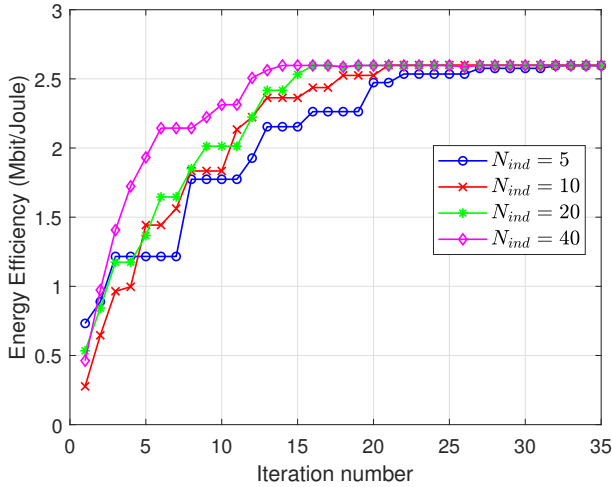


Fig. 2: Energy efficiency versus the iteration number.

TABLE I: Parameter Values Used in the Simulation

Parameter	Value	
M	number of antennas at the BS	16
N_{TR}	number of active transceivers at the BS	4
P_{TR}	circuit power of each active transceiver	30dBm
P_{BS}	circuit power of the BS	35dBm
P_{Tmax}	maximum transmit power at the BS	35dBm
IN	total number of elements on IOSs	120
q_B	location of the BS	$(-50, 5, 5)\text{m}$
K	number of users	40
P_k	circuit power of each user	10dBm
σ^2	noise power	-85dBm
B	bandwidth	1GHz
r_{min}	minimum data rate required	5Mbps
κ	blockage density	0.15blockages/m ²
L_r	room length	10m
W_r	room width	10m
H_r	room height	10m
Ξ	users' spacial distribution	uniform distribution

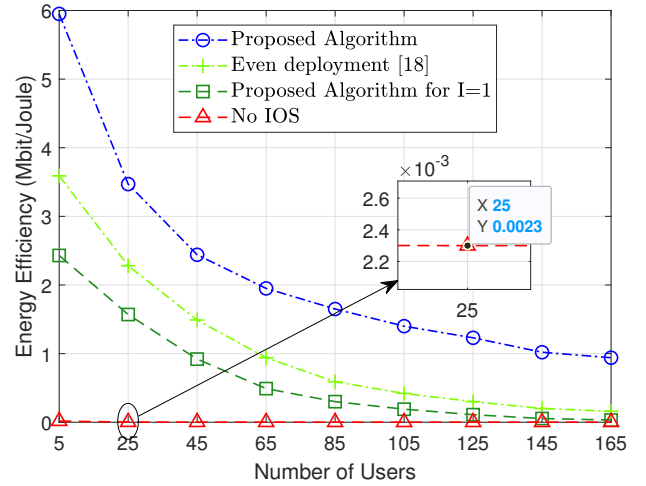


Fig. 3: Energy efficiency versus the number of users.

of users necessitates higher transmit power at the BS. For a specific number of users, the proposed algorithm consistently achieves significantly higher energy efficiency compared to the benchmark schemes. It is noteworthy that the energy efficiency of the BS without deploying any IOS is notably low due to severe penetration losses and attenuations of signal strength at mmWave frequencies.

In Fig. 4, we plot the energy efficiency of the outdoor BS versus the number of users for three different indoor user spatial distributions: (i) the uniform distribution that is considered in the system model; (ii) a Poisson distribution where x_k and y_k of user k ($k = 1, 2, \dots, K$) each follow an independent Poisson distribution with the expected occurrence rate of $\lambda = 3$, i.e., the users are gathered toward the point (3, 3) in the 10m \times 10m room; and (iii) a multivariate normal distribution (MND) where $x_k \sim \mathcal{N}(5, 5)$ and $y_k \sim \mathcal{N}(5, 5)$ for user k ($k = 1, 2, \dots, K$) independently, i.e., the users are gathered around the center point (5, 5) of the room, where the unit of x_k and y_k is meter. For all the three considered

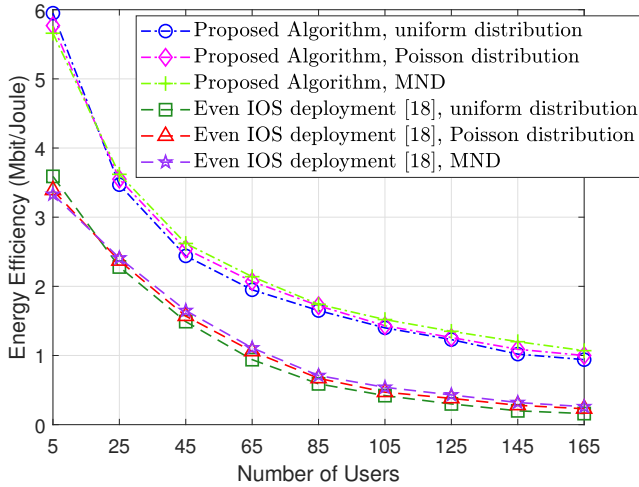


Fig. 4: Energy efficiency versus the number of users for different user distributions.

user distributions, z_k of user k ($k = 1, 2, \dots, K$) follows an independent uniform distribution from 1m to 2m. The figure demonstrates that the proposed algorithm is applicable to different user distributions and is able to achieve a higher BS transmission energy efficiency than the even IOS deployment [18] in all the considered spatial distributions of indoor users.

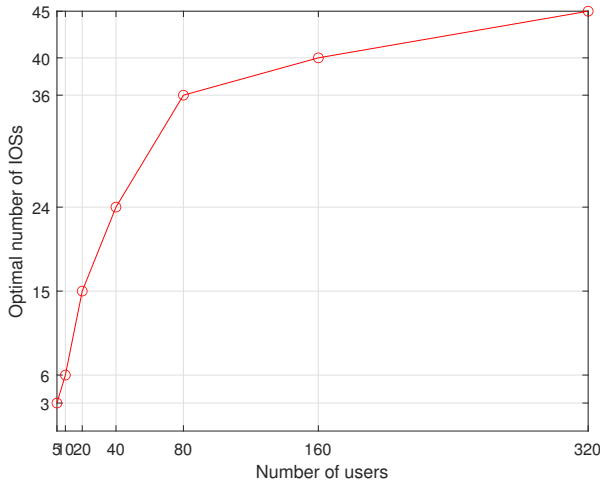


Fig. 5: Optimal number of IOSs versus the number of users.

In Fig. 5, the optimal number of IOSs obtained by Algorithm 2 is plotted against the number of users. The total number of elements of the IOSs is fixed at 360. As the number of users increases, the optimal number of IOSs also increases, albeit at a diminishing rate as the user population grows larger. This trend is attributed to the need for more distributed IOSs to establish LoS links with a larger number of users. However, increasing the number of IOSs while maintaining a fixed total number of elements results in a reduction in the refraction beamforming gain per IOS.

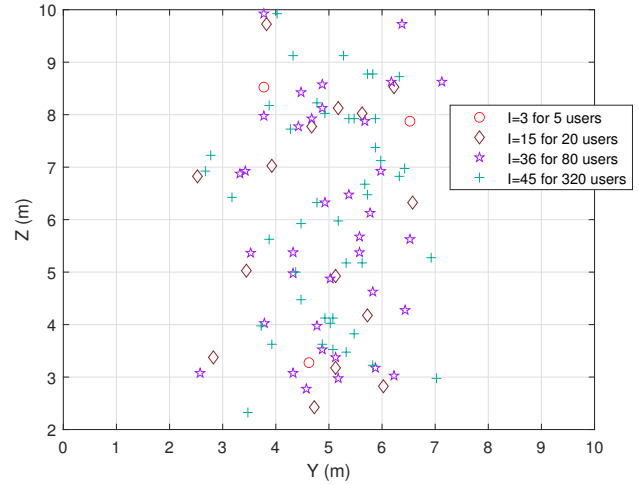


Fig. 6: Optimal number and locations of IOSs and locations.

In Fig. 6, we illustrate the optimal locations of the ideal number of IOSs on the wall for different numbers of users, with a total of 360 elements in the IOSs. Observing the figure, it is evident that, for each considered number of users, the optimized IOS locations converge in the vertical central area of the specified wall. This concentration is attributed to the likelihood that IOSs deployed in the vertical central area are more likely to establish LoS links for a greater number of users compared to those deployed on the left or right side of the wall. Furthermore, the outdoor BS's antenna array is positioned at $(-50, 5, 5)$, facing the center of the wall. Deploying an IOS closer to the center results in a shorter distance from the BS antenna array to the IOS, thereby reducing the path loss of the link. It is noteworthy that some IOSs are deployed above the height of the BS antenna array due to the presence of blockages and the locations of users. In other words, certain IOSs need to be positioned higher than the blockages to establish LoS links for users obstructed by tall obstacles.

In Fig. 7, we depict the transmission energy efficiency of the outdoor BS against the minimum rate requirement of each user. Across all schemes compared, the energy efficiency of the BS decreases as the user rate requirement increases. This trend is attributed to the heightened transmit power needed at the BS to meet the higher minimum rate requirement, resulting in a reduction in energy efficiency. Notably, the proposed algorithm consistently outperforms the other schemes for each considered value of the user rate requirement due to the optimized number and locations of IOSs.

In Fig. 8, we illustrate the transmission energy efficiency of the outdoor BS against the blockage density. Across all considered schemes, the energy efficiency of the BS experiences a decline with increasing blockage density. This decline is attributed to the reduction in LoS links between the IOSs and the users as the blockage density rises. The proposed algorithm outperforms the other schemes significantly due to the optimized number and locations of IOSs, ensuring a

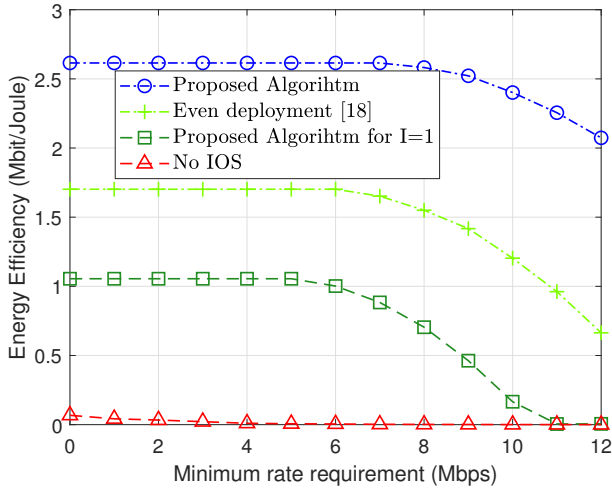


Fig. 7: Energy efficiency versus minimum rate requirement per user.

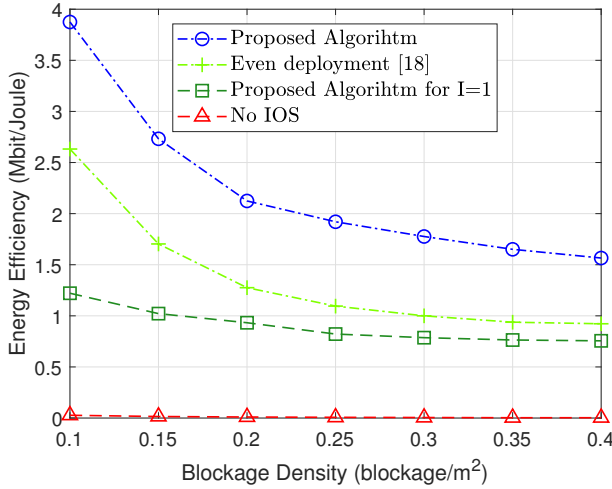


Fig. 8: Energy efficiency versus the blockage density.

larger number of LoS links between the IOSs and the users. The performance gap between the centralized IOS deployment scheme and the proposed algorithm/even deployment scheme becomes smaller for higher blockage densities. This is because, under scenarios of the proposed algorithm/even deployment scheme, the number of LoS links significantly decreases with the increase in blockage density. In contrast, for the centralized IOS deployment scheme, the decrease is slight since many LoS links have already been blocked even for a small blockage density.

In Fig. 9, we present the transmission energy efficiency of the outdoor BS against the total number of elements on the IOSs for the three IOS deployment schemes. Notably, for each scheme, the BS’s energy efficiency increases with the total number of elements on the IOSs, as the channel gain of the IOSs grows with the total number of elements. For a given

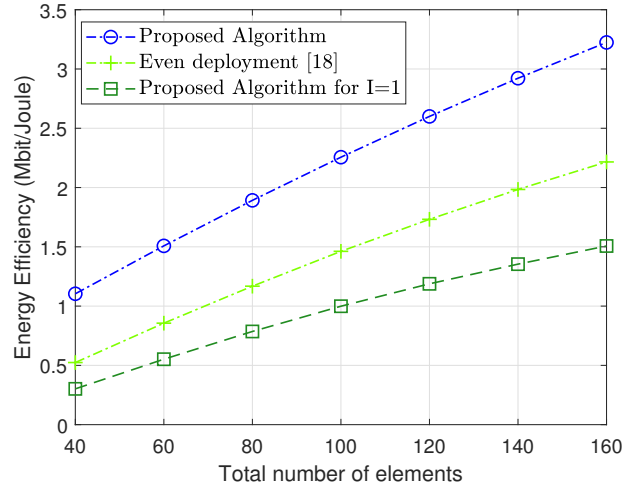


Fig. 9: Energy efficiency versus IOSs’ total number of elements.

total number of elements, the proposed algorithm consistently achieves the highest energy efficiency for the BS, followed by the evenly distributed IOS deployment [18]. The centralized IOS deployment (i.e., the proposed algorithm with $I = 1$) achieves the lowest energy efficiency for the BS. This order is attributed to the proposed algorithm having the most LoS links between the IOSs and the users, enhancing the utilization of the increased elements in the IOSs, while the centralized IOS deployment scheme has the fewest LoS links.

V. CONCLUSION AND FUTURE WORK

In this study, we explored the dynamics of multiple IOSs in outdoor-to-indoor mmWave communications for multiple indoor users in the presence of indoor blockages. To maximize the transmission energy efficiency of the outdoor BS while ensuring each user’s downlink data rate surpasses a specified threshold, we introduced the EEM algorithm and the IOSLN algorithm. These algorithms jointly optimize the number, locations, and phase shifts of IOSs, along with the beamforming vectors of the BS. Simulation results demonstrate that the proposed algorithms significantly enhance the downlink energy efficiency of the BS compared to benchmark schemes that either neglect IOS deployment or do not optimize the number or locations of IOSs. The optimized number and locations of IOSs play a crucial role in maximizing LoS links to users. The optimal number of IOSs increases with the number of users, but the rate of increase diminishes as the user population expands. This is attributed to the trade-off, as distributing a fixed total number of refracting elements to an increasing number of IOSs results in a reduced refraction beamforming gain per IOS. Optimal IOS locations concentrate in the vertical central area of the wall. This strategic placement allows central IOSs to create LoS links for more users compared to those on the left or right sides. Additionally, central IOSs are closer to the outdoor BS, which faces the center of the wall.

Furthermore, the transmission energy efficiency of the BS exhibits a positive correlation with the total number of IOS elements but experiences decreases with the number of users, user rate requirements, and blockage density. These findings provide valuable insights into optimizing multiple IOSs for efficient outdoor-to-indoor mmWave communications.

In our future studies, we plan to extend this work to more complex scenarios, where an outdoor BS provides services to both outdoor and indoor mobile users. Such scenarios will necessitate the use of IOSs' capabilities of both reflecting and refracting incident signals, while considering the dynamic channel conditions and potentially different mobility patterns of outdoor and indoor users. This approach promises to unveil interesting possibilities for enhancing communication efficiency and user experience.

REFERENCES

- [1] ABI Research, "ABI research anticipates in-building mobile data traffic to grow by more than 600% by 2020," Jan. 2016.
- [2] A. Schumacher, R. Merz and A. Burg, "A mmWave bridge concept to solve the cellular outdoor-to-indoor challenge," 2020 IEEE 91st Vehicular Technology Conference (VTC2020-Spring), Antwerp, Belgium, 2020, pp. 1-6.
- [3] G. Larson, "Deployment options for providing indoor coverage in high frequency bands," Master Thesis, KTH Royal Institute of Technology, Stockholm, 2015.
- [4] D. W. K. Ng, M. Breiling, C. Rohde, F. Burkhardt and R. Schober, "Energy-efficient 5G outdoor-to-indoor communication: SUDAS over licensed and unlicensed spectrum," in IEEE Transactions on Wireless Communications, vol. 15, no. 5, pp. 3170-3186, May 2016.
- [5] C. Umit Bas et al., "Outdoor to indoor propagation channel measurements at 28 GHz," in IEEE Transactions on Wireless Communications, vol. 18, no. 3, pp. 1477-1489, Mar. 2019.
- [6] M. Xiao et al., "Millimeter wave communications for future mobile networks," in IEEE Journal on Selected Areas in Communications, vol. 35, no. 9, pp. 1909-1935, Sept. 2017.
- [7] J. Lee, K. Kim, M. Kim and J. Park, "32-GHz outdoor-to-indoor channel measurement of propagation losses and delay spread," 2019 IEEE International Symposium on Antennas and Propagation and USNC-URSI Radio Science Meeting, Atlanta, GA, USA, pp. 2071-2072, Jul. 2019.
- [8] A. B. Zekri, R. Ajjou, A. Chemsas and S. Ghendir, "Analysis of outdoor to indoor penetration loss for mmWave channels," 2020 1st International Conference on Communications, Control Systems and Signal Processing (CCSSP), El Oued, Algeria, pp. 74-79, May 2020.
- [9] M. I. Rochman, V. Sathya and M. Ghosh, "Outdoor-to-indoor performance analysis of a commercial deployment of 5G mmWave," 2022 IEEE Future Networks World Forum (FNWF), Montreal, QC, Canada, pp. 519-525, Oct. 2022.
- [10] K. Ntontin and C. Verikoukis, "Relay-aided outdoor-to-indoor communication in millimeter-wave cellular networks," in IEEE Systems Journal, vol. 14, no. 2, pp. 2473-2484, Jun. 2020.
- [11] R. Liang, J. Fan, H. Liu, Y. Ge and J. Zhang, "Dual-hop hybrid IRS-aided outdoor-to-indoor mmWave communications," in IEEE Communications Letters, vol. 26, no. 12, pp. 2979-2983, Dec. 2022.
- [12] H. Zhang et al., "Intelligent omni-surfaces for full-dimensional wireless communications: Principles, technology, and implementation," in IEEE Communications Magazine, vol. 60, no. 2, pp. 39-45, Feb. 2022.
- [13] Y. Zhang, B. Di, H. Zhang, Z. Han, H. V. Poor and L. Song, "Meta-wall: Intelligent omni-surfaces aided multi-cell MIMO communications," in IEEE Transactions on Wireless Communications, vol. 21, no. 9, pp. 7026-7039, Sept. 2022.
- [14] S. Zeng, H. Zhang, B. Di and L. Song, "Reconfigurable refractive surface-enabled multi-user holographic MIMO communications," in IEEE Transactions on Wireless Communications, Oct. 2023.
- [15] V. Singh, M. Khalily, S. B. Amlashi, J. D. Carey and R. Tafazolli, "Fully-transparent transmission surface for outdoor-indoor mmWave coverage enhancement," 2020 International Conference on UK-China Emerging Technologies (UCET), Glasgow, UK, pp. 1-4, Aug. 2020.
- [16] M. Nemati, B. Maham, S. R. Pookhrel and J. Choi, "Modeling RIS empowered outdoor-to-indoor communication in mmWave cellular networks," in IEEE Transactions on Communications, vol. 69, no. 11, pp. 7837-7850, Nov. 2021.
- [17] X. Xie, C. He, X. Ma, F. Gao, Z. Han and Z. J. Wang, "Joint precoding for active intelligent transmitting surface empowered outdoor-to-indoor communication in mmWave cellular networks," in IEEE Transactions on Wireless Communications, vol. 22, no. 10, pp. 7072-7086, Oct. 2023.
- [18] Z. Li, H. Hu, J. Zhang and J. Zhang, "Coverage analysis of multiple transmissive RIS-aided outdoor-to-indoor mmWave networks," in IEEE Transactions on Broadcasting, vol. 68, no. 4, pp. 935-942, Dec. 2022.
- [19] S. Zhang et al., "Intelligent omni-surfaces: Ubiquitous wireless transmission by reflective-refractive metasurfaces," in IEEE Transactions on Wireless Communications, vol. 21, no. 1, pp. 219-233, Jan. 2022.
- [20] T. Bai, R. Vaze, and R. W. Heath, "Analysis of blockage effects on urban cellular networks," IEEE Trans. Wireless Commun., vol. 13, no. 9, pp. 5070-5083, Sept. 2014.
- [21] Z. Yang, J. Shi, Z. Li, M. Chen, W. Xu and M. Shikh-Bahaei, "Energy efficient rate splitting multiple access (RSMA) with reconfigurable intelligent surface," 2020 IEEE International Conference on Communications Workshops (ICC Workshops), pp. 1-6, Jun. 2020.
- [22] L. You, J. Xiong, D. W. K. Ng, C. Yuen, W. Wang and X. Gao, "Energy efficiency and spectral efficiency tradeoff in RIS-aided multiuser MIMO uplink transmission," in IEEE Transactions on Signal Processing, vol. 69, pp. 1407-1421, Dec. 2021.
- [23] S. Boyd and L. Vandenberghe, Convex optimization. Cambridge University Press, 2004.
- [24] W. Dinkelbach, "On nonlinear fractional programming," Management Science, vol. 13, no. 7, pp. 492-498, Mar. 1967.
- [25] M. S. Lobo, L. Vandenberghe, S. Boyd, and H. Lebret, "Applications of second-order cone programming," Linear algebra and its applications, vol. 284, no. 1-3, pp. 193-228, Nov. 1998.
- [26] M. Grant, S. Boyd, and Y. Ye, "CVX: Matlab software for disciplined convex programming," 2008.
- [27] M. Sebag and A. Ducoulombier, "Extending population-based incremental learning to continuous search spaces," International Conference on Parallel Problem Solving from Nature, pp. 418-427, Sept. 1998.